Electronic Supplementary Material (ESI) for Journal of Materials Chemistry A.

Supporting Information

Ultrasensitive micro/nanocrack-based graphene nanowall strain sensors derived from the substrate's Poisson's ratio effect

Hongyan Sun,[a,b,c] Chen Ye,[a,b] Gang Zhao,[d] Huan Zhang,[d] Zhiduo Liu,[a] Wen Dai,[a,b] Junjie Wang,[d] Fakhr E. Alam,[e] Qingwei Yan,[a] Xinming Li,[f] Jian Xu,[d] Chin-Yin Chen,[d] Pei Zhao,[g] Jichun Ye,[d] Nan Jiang,[a] Ding Chen,*[h] Sudong Wu,*[i] Jing Kong,[j] Cheng-Te Lin*[a,b]

[a] Key Laboratory of Marine Materials and Related Technologies, Zhejiang Key Laboratory of Marine Materials and Protective Technologies, Ningbo Institute of Materials Technology and Engineering (NIMTE), Chinese Academy of Sciences, Ningbo 315201, P.R. China. E-mail: linzhengde@nimte.ac.cn

[b] Center of Materials Science and Optoelectronics Engineering, University of Chinese Academy of Sciences, Beijing 100049, P.R. China

[c] Bionic Sensing and Intelligence Center (BSIC), Institute of Biomedical and Health Engineering, Shenzhen Institutes of Advanced Technology, Chinese Academy of Science, 1068 Xueyuan Avenue, Shenzhen 518055, P.R. China

[d] Ningbo Institute of Materials Technology and Engineering, Chinese Academy of Sciences, Ningbo 315201, China.

[e] Department of physics, University of Wah, Quaid Avenue, Wah Cantt, Pakistan

[f] Guangdong Provincial Key Laboratory of Nanophotonic Functional Materials and Devices, School of Information and Optoelectronic Science and Engineering, South China Normal University, Guangzhou 510006 China

[g] Center for X-Mechanics and Institute of Applied Mechanics, Zhejiang University, Hangzhou 310012, P. R. China

[h] State Key Laboratory of Advanced Design and Manufacturing for Vehicle Body, College of Mechanical and Vehicle Engineering, Hunan University, 410082 Changsha, P.R. China. E-mail: chending@hnu.edu.cn

[i] Academy for Advanced Interdisciplinary Studies, Southern University of Science and Technology, Shenzhen 518055, P.R. China. E-mail: wusd@sustech.edu.cn

[j] Department of Electrical Engineering and Computer Science, Massachusetts Institute of Technology, Cambridge, Massachusetts, 02139, United States

Fig. S1–S9, Video S1–S3, and Table S1

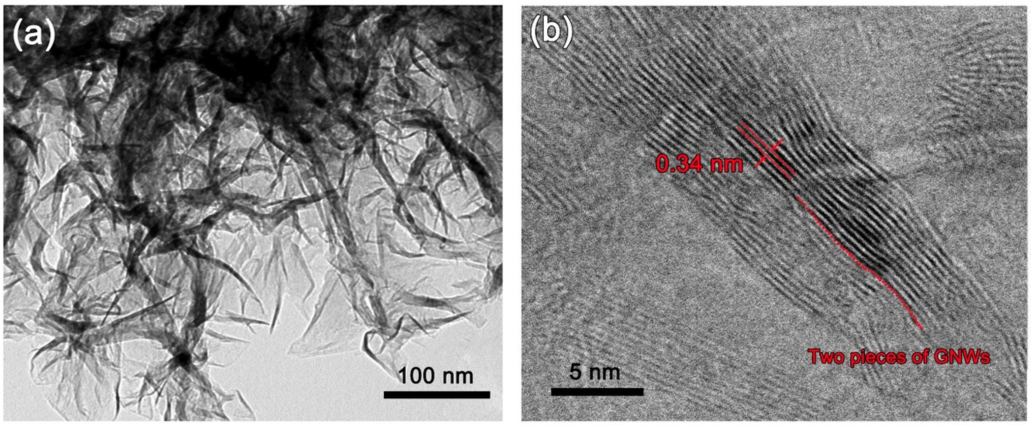

Fig. S1 (a) TEM and (b) high-resolution TEM images of GNWs.

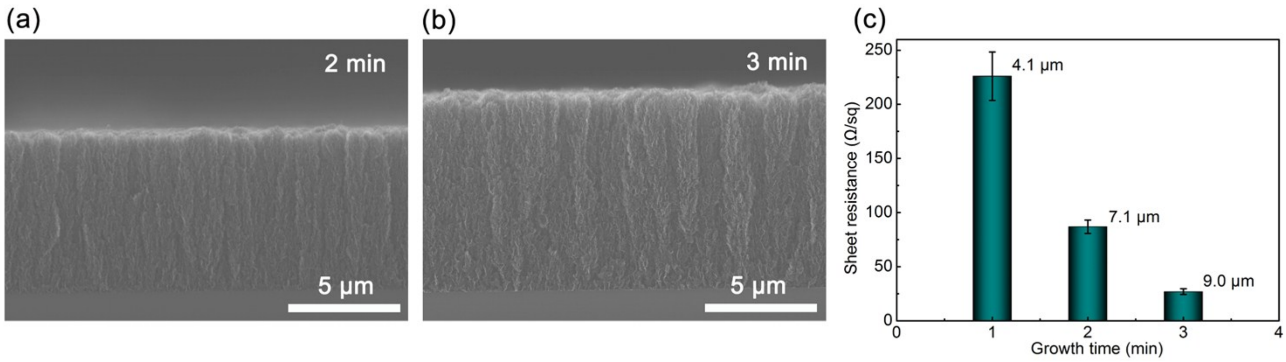

Fig. S2 Cross-sectional SEM images of GNWs after (a) 2-min and (b) 3-min growth. (c) The sheet resistance of GNWs as a function of growth time and film thickness.

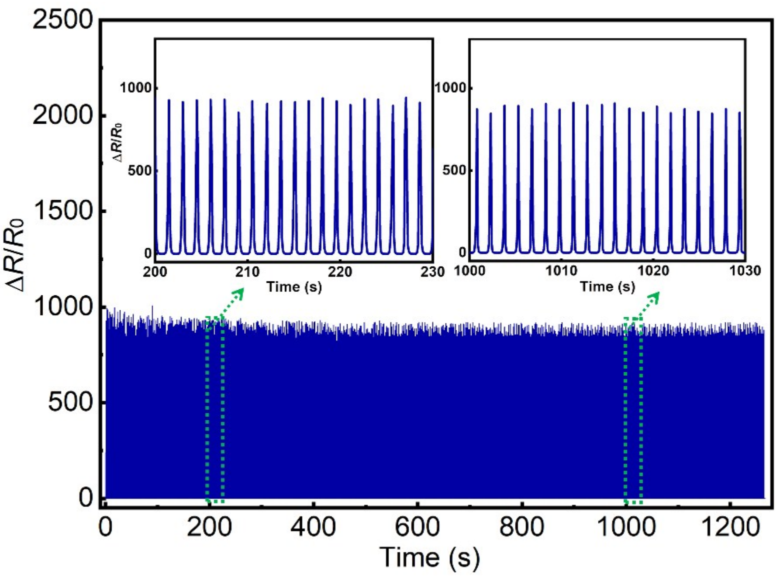

Fig. S3 Durability test of GNWs strain sensors under repeated stretching/releasing cycles (0% – 3%) for over 800 times.

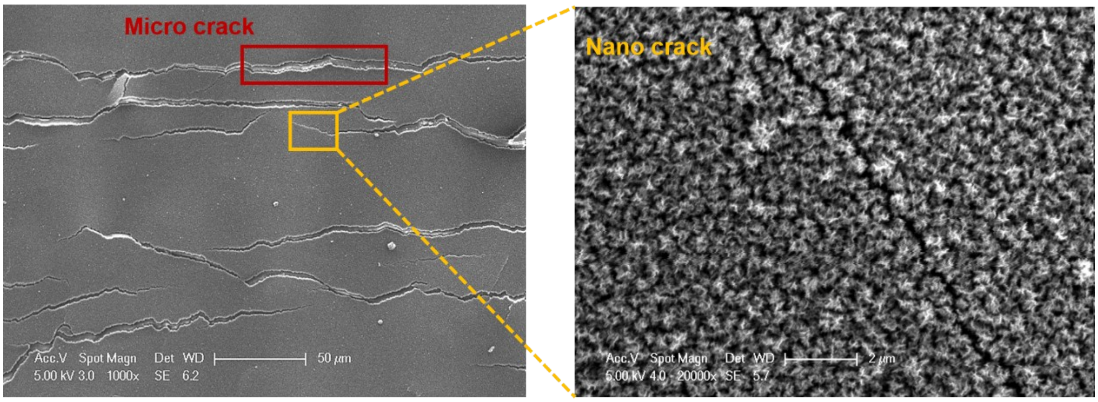

Fig. S4 SEM image exhibiting the micro/nanocracks in the GNW structure during stretching.

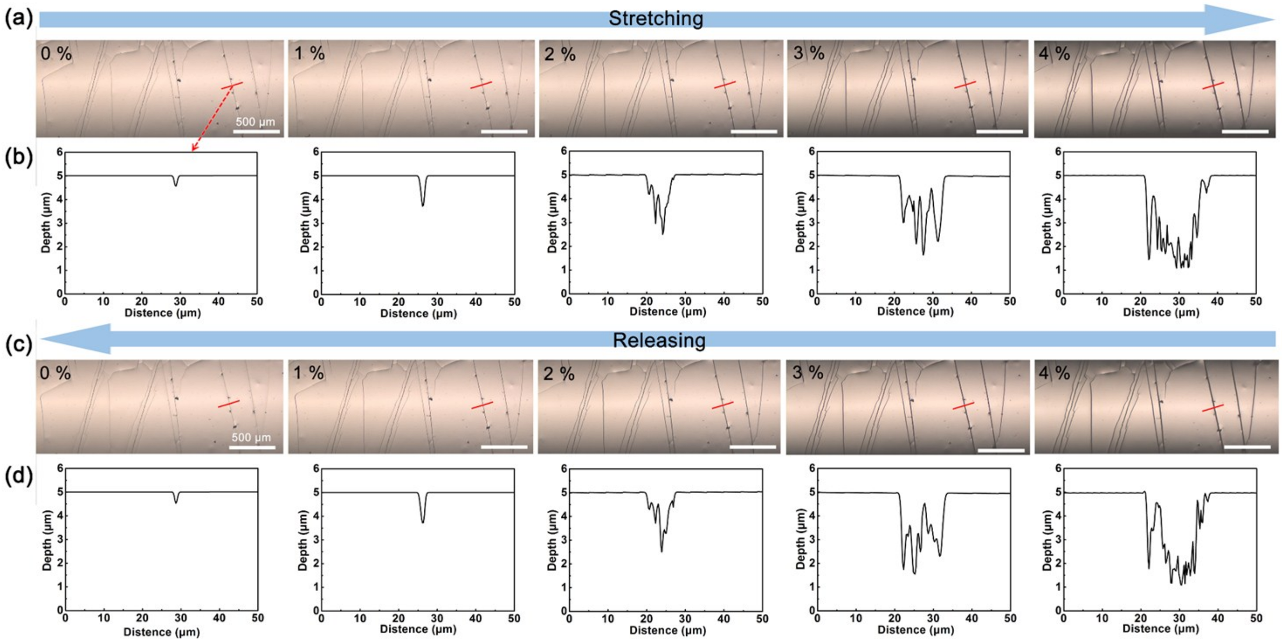

Fig. S5 The formation and evolution of microcracks under stretching from 0% to 4% strains: (a) OM images and (b) the width/depth profiles. (c) (d) The functional and morphological recovery of microcracks during strain release.

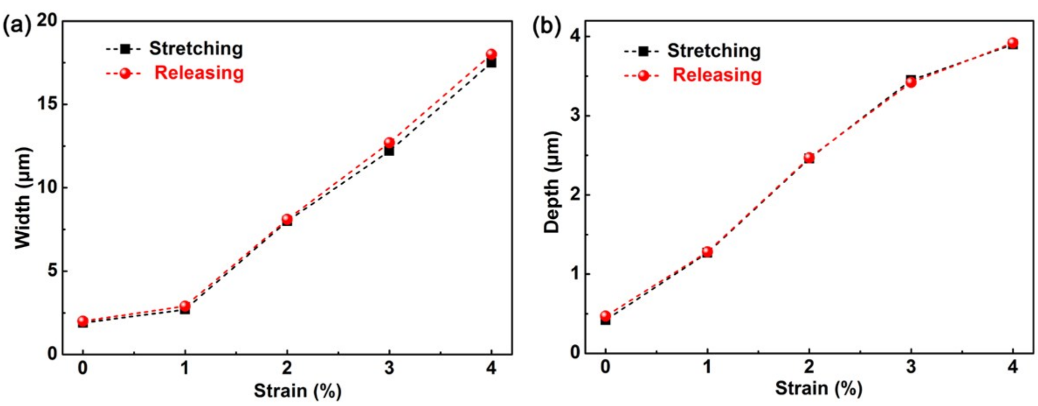

Fig. S6 The evolution of (a) width and (b) depth of microcracks under stretching and recovery.

Microcrack Evolution Monitoring. The microcrack evolution in the GNW structure was monitored during uniaxial stretching and releasing. As the results shown in **Fig. S4** and **S5**, the OM images and depth profiles indicate that both the gap width and depth of microcracks increase as the applied strain increases step by step until 4%, whereas the number of microcracks remains the same. When the strain is released, the gap width and depth correspondingly decrease and the microcracks can be recovered to the original level.

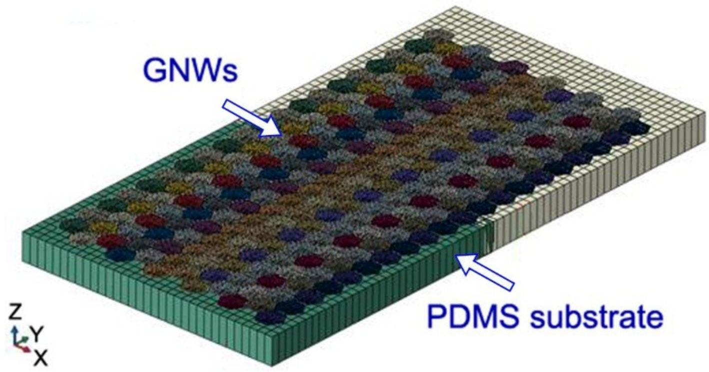

Fig. S7 Finite element model of GNW strain sensors placed on the PDMS substrate.

Finite Element Simulation Setup. In order to study Poisson's ratio effect of PDMS substrate on the mechanosensitivity of GNW strain sensors under tensile load, we developed a finite element model composed of GNWS and the substrate using 4-node bilinear plane stress quadrilateral with reduced integration and hourglass control (CPS4R). The GNW films were comprised of 240 GNW building blocks with a hexagonal shape, as presented in **Fig. S6**. The finite element model containing 20178 elements and 24152 nodes in total was solved using ABAQUS/Standard (ABAQUS Inc., USA). Considering that the thickness of GNW films is far less than that of the substrate, the "mesh superposition technique" was employed for model development. In this configuration, GNW mesh was embedded into the host mesh (PDMS substrate) and the kinematic constrains are introduced between the nodes of embedded and host elements. The translational degrees of freedom of embedded nodes are interpolated using the values of degrees of freedom of surrounding host nodes. Due to the relatively high Poisson's ratio (≈ 0.48) of PDMS substrate, GNW films were stretched in the longitudinal direction (Y-axis) meanwhile compressed in the horizontal direction (X-axis) at an applied strain. As the simulation results shown in **Video S2**, the adjacent GNWs slide along the boundary during stretching, resulting in an abrupt decrease of electrical contact areas and junctions. Because the electrical resistance of the devices is inversely proportional to the contact areas and junctions, we conclude that the ultrahigh mechanosensitivity of GNW strain sensors can be attributed to the relative motion between GNW building blocks derived from substrate Poisson's ratio effect.

Video S1. The nanocrack evolution based on the relative motion between GNW building blocks assuming Poisson's ratio of the substrate is zero.

Video S2. The nanocrack evolution derived from Poisson's ratio effect of PDMS substrate.

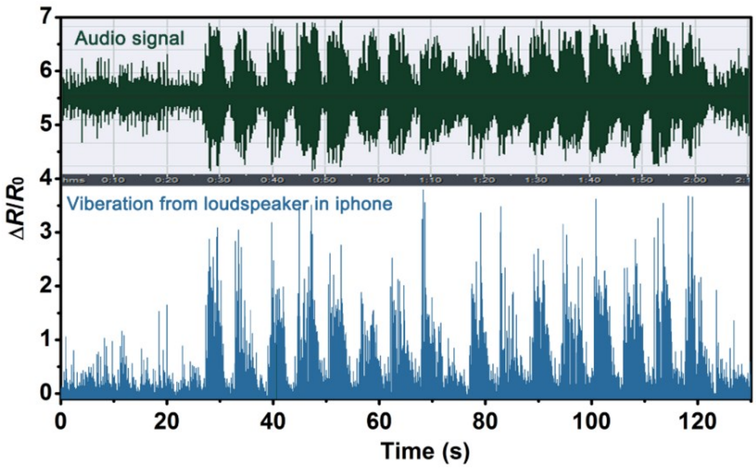

Fig. S8 GNW strain sensors applied to the detection of acoustic waveforms generated from a loudspeaker.

Video S3. The video of arterial pulse waveforms.

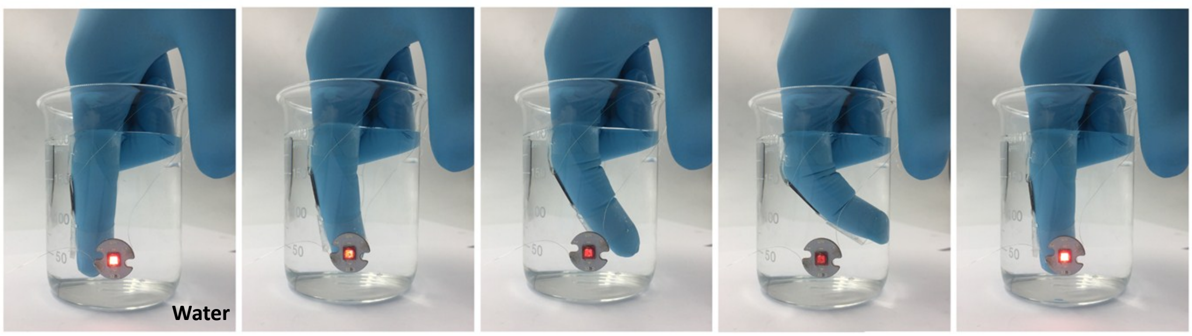

Fig. S9 GNW strain sensors applied to modulate the LED brightness in underwater environment.

Table S1. The gauge factor of graphene-based strain sensors reported in the literature (the applied strain range: < 10%). The abbreviation of graphene oxide and reduced graphene oxide is GO and rGO, respectively.

Materials	Max GF	Strain (%)	References
Graphene films:			
CVD-grown graphene	6.1	1	Nano Lett. 2010, 10, 490

Spray coated graphene films	≈ 14	1.7	Nano Lett. 2012, 12, 5714
CVD-grown graphene	14	7.1	Carbon 2013, 51, 236
GO reduced by laser scribing	9.4	≈ 10	Nanoscale 2014, 6, 699
GO reduced by laser scribing	673	5	ACS Nano 2018, 12, 8839
Laser-induced graphene	≈ 40	≈ 1.5	Adv. Funct. Mater. 2018, 1805271
Laser-induced graphene	316.3	9 – 11	Adv. Funct. Mater. 2019, 1904706
Nanographene films	600	< 2	ACS Nano 2015, 9, 1622
Exfoliated graphene films	4383	3.4	Adv. Funct. Mater. 2016, 26, 1322
Graphene sheets	500	1	Science 2016, 354, 1257
Graphene sheets	400	7.5	Nanoscale 2016, 8, 20090
Graphene nanosheets	150	≈ 0.6	Adv. Mater. Technol. 2019, 1800572
rGO	261	2	ACS Appl. Mater. Interfaces 2016, 8, 22501
Graphene woven fabrics:			
	≈ 1.0×10^3	6	Adv. Funct. Mater. 2014, 24, 4666
	≈ 1.0×10^4	8	ACS Nano 2015, 9, 10867
	223	3	Mater. Horiz. 2017, 4, 477
rGO-coated glass fabric/silicone composite	≈ 113	≈ 4	ACS Appl. Mater. Interfaces 2018, 10, 35503
Graphene-Silk Fabric	124	10	Adv. Mater. Interfaces 2020, 7, 1901507
3D graphene:			
Graphene foam composites	98.6	5	ACS Appl. Mater. Interfaces 2016, 8, 18954
Graphene aerogel nanocomposites	61.3	10	ACS Appl. Mater. Interfaces 2016, 8, 24853
3D-porous graphene	27	4	ACS Appl. Nano Mater. 2020, 3, 283

Graphene-based composites:			
GO ribbons	≈ 1000	7.5	ACS Nano 2015, 9, 12320
Graphene/poly(vinyl alcohol) fibers	50	6.3	Chem. Mater. 2015, 27, 6969
rGO-paper	8	0.4	Adv. Funct. Mater. 2018, 1806057
Silver nanowires bridging graphene	323	5	Carbon 2020, 156, 253
Graphene nanowalls	8.6×10^{4}	≈ 4	**This work**